




Article

Double-Diffusive Convection in Bidispersive Porous Medium with Coriolis Effect

Chirnam Ramchandraiah¹, Naikoti Kishan¹ , Gundlapally Shiva Kumar Reddy² , Kiran Kumar Paidipati³ 
and Christophe Chesneau^{4,*}

¹ Department of Mathematics, Osmania University, Hyderabad 500007, India; ramchandaryadav567@gmail.com (C.R.); kishan_n@osmania.ac.in (N.K.)

² Department of Applied Sciences, National Institute of Technology Goa, Ponda 403401, India; gshivakumarreddy913@nitgoa.ac.in

³ Area of Decision Sciences, Indian Institute of Management Sirmaur, Sirmaur 173025, India; kkpaidipati@iimsirmaur.ac.in

⁴ Department of Mathematics, LMNO, CNRS-Université de Caen, Campus II, Science 3, CEDEX, 14032 Caen, France

* Correspondence: christophe.chesneau@gmail.com

Abstract: In this paper, the thermal instability of rotating convection in a bidispersive porous layer is analyzed. The linear stability analysis is employed to examine the stability of the system. The neutral curves for different values of the physical parameters are shown graphically. The critical Rayleigh number is evaluated for appropriate values of the other governing parameters. Among the obtained results, we find: the Taylor number has a stabilizing effect on the onset of convection; the Soret number does not show any effect on oscillatory convection, as the oscillatory Rayleigh number is independent of the Soret number; there exists a threshold, $R_c^* \in (0.45, 0.46)$, for the solute Rayleigh number, such that, if $R_c > R_c^*$, then the convection arises via an oscillatory mode; and the oscillatory convection sets in and as soon as the value of the Soret number reaches a critical value, ($\in (0.6, 0.7)$), and the convection arises via stationary convection.



Citation: Ramchandraiah, C.; Kishan, N.; Reddy, G.S.K.; Paidipati, K.K.; Chesneau, C. Double-Diffusive Convection in Bidispersive Porous Medium with Coriolis Effect. *Math. Comput. Appl.* **2022**, *27*, 56. <https://doi.org/10.3390/mca27040056>

Received: 22 May 2022

Accepted: 27 June 2022

Published: 30 June 2022

Publisher's Note: MDPI stays neutral with regard to jurisdictional claims in published maps and institutional affiliations.



Copyright: © 2022 by the authors. Licensee MDPI, Basel, Switzerland. This article is an open access article distributed under the terms and conditions of the Creative Commons Attribution (CC BY) license (<https://creativecommons.org/licenses/by/4.0/>).

Keywords: bidispersive porous media; thermal convection; linear stability analysis

1. Introduction

In recent years, great attention has been devoted to the thermal instability in bidispersive porous medium (BDPM). A BDPM is an extension of a regular porous medium. In general, it is considered a regular porous medium where the solid phase is replaced by another porous medium. A BDPM is composed of clusters of large particles that are agglomerations of small particles [1,2]. The voids between the clusters are known as macropores, and the voids within the clusters are known as micropores. In other words, a BDPM is a porous medium in which fractures or tunnels have been introduced. In the present model, the f-phase and p-phase are represented by 'fracture phase' and 'porous phase', respectively. Understanding convection in a BDPM is of considerable interest for geophysical applications [3,4]. The theory of thermal convection in a BDPM was developed by Nield and Kuznetsov [5–11], Kuznetsov and Nield [12], and Straughan [13,14]. All these authors considered two different velocities and two different temperatures in the macro and micro pores. In their analysis, they found that, in a BDPM, the critical values of Rayleigh numbers are much larger than those in the regular porous medium. Later, much research made an effort to investigate the convective instability in a BDPM.

Very recently, Falsaperla et al. [15] and Gentile and Straughan [16,17] studied the same problem by using a single equation for temperature. In particular, Gentile and Straughan [16,17] analyzed the non-linear stability theory for the problem of thermal convection in a BDPM. They proved that the linear and non-linear stability thresholds

coincide. Very recently, Capone et al. [18] have shown that the linear instability and non-linear stability thresholds for the problem of thermal instability in a rotating BDPM are different. Later, Capone and De Luca [19] extended their work by considering inertia terms, and they showed that the effect of the Vadasz number can give rise to an oscillatory mode at the loss of stability of a thermal motionless state.

On the other hand, double-diffusive instability in porous media is an interesting subject of research due to its applications in different industries, such as the migration of solutes in watersaturated soils, the spread of pollutants, drying processes, evaporative cooling of high-temperature systems, and solar ponds [8]. The study of thermosolutal convection of a fluidsaturated porous medium has attracted the attention of many researchers [20–28]. In addition, Straughan [29] developed a model for double-diffusive convection in a BDPM. Later, Straughan [30] extended this work by considering the effect of inertia. He showed that the inertia term had a very strong effect on the double-diffusive convection in a BDPM. Badday and Harfash [31] have studied the double-diffusive convection in BDPM with chemical reaction and magnetic field effects.

In this paper, the coriolis effect on thermosolutal convection in a rotating bidisperse porous layer is studied. We reconsider the problem investigated in [18] in light of the Soret effect. The plan of the article is as follows. Section 2 describes the mathematical problem. In Section 3, we describe the linear stability analysis. The critical values of Rayleigh numbers at the onset of stationary and oscillatory convection are determined. The results and discussions are presented in Section 4, which contains a table to provide some examples in which stationary or oscillatory instability sets in, and figures showing the neutral stability curves for steady and oscillatory instability. The paper ends with a conclusion part in Section 5.

2. Mathematical Formulation

Let us consider a horizontal fluid saturated bidisperse porous layer confined between $z = 0$ and $z = d$. In this setting, let V_i^f and V_i^p be the velocity of the fluid in the macro pores and the velocity of the fluid in the micro pores, respectively. The fixed temperatures at $z = 0$ and at $z = d$ are $T_L^0 C$ and $T_U^0 C$, respectively, with $T_L > T_U > 0$. It is rotating at a constant rate Ω . The axis of rotation is parallel to z -axis. The Boussinesq approximation is used to account for the density variations.

The hydrodynamic model representing flow behavior in bidisperse porous layer differs from the classical porous layer theory by exhibiting two different pressures in the pores, following the multiporosity model. The flow within each type of pores is determined by its own pressure gradient through Darcy’s law. Hence, four additional equations corresponding to the micro-pores are considered to make the relevant equations for mass and momentum balances closed. The governing equations consist of the momentum and continuity equations (see the references [18,31], and the visual representation in Figure 1). By adopting the Boussinesq approximation in the macro and micro pores, these equations can be written as

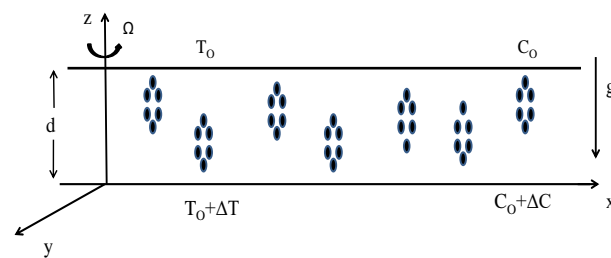


Figure 1. Physical Configuration.

$$\nabla \cdot \mathbf{V}^f = 0, \nabla \cdot \mathbf{V}^p = 0, \tag{1}$$

$$-\frac{\mu}{\kappa_f} \mathbf{V}^f - \delta(\mathbf{V}^f - \mathbf{V}^p) - \nabla P^f - \rho g \hat{e}_z - \frac{2\rho_0 \Omega}{\delta} \hat{e}_z \times \mathbf{V}^f = 0, \tag{2}$$

$$-\frac{\mu}{\kappa_p} \mathbf{V}^p - \delta(\mathbf{V}^p - \mathbf{V}^f) - \nabla P^p - \rho g \hat{e}_z - \frac{2\rho_0 \Omega}{\epsilon} \hat{e}_z \times \mathbf{V}^p = 0. \tag{3}$$

Then, we consider a linear relation for the density of form

$$\rho = \rho_0 [1 - \alpha(T - T_0) + \alpha_c(C - C_0)]. \tag{4}$$

The equation of the energy balance can be written as

$$(\rho c)_m \frac{\partial T}{\partial t} + (\rho c)_f (\mathbf{V}^f + \mathbf{V}^p) \cdot \nabla T = k_m \nabla^2 T, \tag{5}$$

where c is the specific heat in the porous medium. The coefficients $(\rho c)_m$ and k_m are given by

$$(\rho c)_m = (1 - \epsilon)(1 - \delta)(\rho c)_s + [\delta + \epsilon(1 - \delta)](\rho c)_f, \tag{6}$$

$$k_m = (1 - \epsilon)(1 - \delta)k_s + [\delta + \epsilon(1 - \delta)]k_f. \tag{7}$$

The equation for the concentration field taking into account the Soret effect on the diffusion coefficient can be written as

$$\epsilon_1 \frac{\partial C}{\partial t} + (\mathbf{V}^f + \mathbf{V}^p) \cdot \nabla C = \epsilon_2 \nabla^2 C + \hat{S} \nabla^2 T, \tag{8}$$

where

$$\epsilon_1 = \delta + \epsilon(1 - \delta), \tag{9}$$

$$\epsilon_2 = \delta k_c^f + \epsilon(1 - \delta)k_c^p, \tag{10}$$

$$\hat{S} = \phi S_T^f + \epsilon(1 - \phi)S_T^p, \tag{11}$$

subject to the boundary conditions

$$\mathbf{V}^f \cdot \hat{e}_z = \mathbf{V}^p \cdot \hat{e}_z = 0, \text{ on } z = 0, d, \tag{12}$$

$$T(x, y, 0, t) = T_L, T(x, y, d, t) = T_U \quad (T_L > T_U), \tag{13}$$

$$C(x, y, 0, t) = C_L, C(x, y, d, t) = C_U \quad (C_L > C_U). \tag{14}$$

The basic state solution is then

$$\mathbf{V}_b^f = 0, \mathbf{V}_b^p = 0, T_b = T_L - \beta z, C_b = C_L - \beta_c z, \tag{15}$$

where $\beta = \frac{T_L - T_U}{d}$ and $\beta_c = \frac{C_L - C_U}{d}$.

Let $\mathbf{V}^f, \mathbf{V}^p, P^f, P^p, T,$ and C be a perturbation to the steady Equation (15).

The perturbations are non-dimensional, with length scale $d,$ velocity scale $V,$ time scale $\tau,$ temperature scale $T^*,$ and concentration scale $C^*,$ where

$$\tau = \frac{(\rho c)_m d^2}{k_m}, \quad V = \frac{k_m}{(\rho c)_f d},$$

$$T^* = \frac{\beta V (\rho c)_f d^2}{k_m}, \quad C^* = \frac{\beta_c V d^2}{\epsilon_2}.$$

Define the quantities $\gamma, \kappa_r, A, \eta, R, R_C, Ta, Le,$ and S by

$$\begin{aligned} \gamma &= \frac{\delta\kappa_f}{\mu}, & \kappa_r &= \frac{\kappa_f}{\kappa_p}, & \omega &= \frac{(\rho c)_m}{(\rho c)_f}, \\ Ta &= \frac{2\rho_0\Omega\kappa_f}{\mu\phi}, & R &= \frac{\rho_0\beta g\alpha d^2(\rho c)_f\kappa_f}{\mu k_m}, & R_C &= \frac{\rho_0\beta_c g\alpha_c d^2\kappa_f}{\mu\epsilon_2}, \\ Le &= \frac{k_m}{(\rho c)_m\epsilon_2}, & S &= \frac{\hat{S}T^*}{\epsilon_2 C^*}. \end{aligned}$$

All these quantities have been explained in the nomenclature. The non-dimensional equations (after omitting the asterisks) governing the system are

$$\nabla \cdot \mathbf{V}^f = 0, \nabla \cdot \mathbf{V}^p = 0, \tag{16}$$

$$-\mathbf{V}^f - \gamma(\mathbf{V}^f - \mathbf{V}^p) - \nabla P^f + (R\theta - R_C\phi)\hat{e}_z - Ta\hat{e}_z \times \mathbf{V}^f = 0, \tag{17}$$

$$-\kappa_r\mathbf{V}^p - \gamma(\mathbf{V}^p - \mathbf{V}^f) - \nabla P^p + (R\theta - R_C\phi)\hat{e}_z - \eta Ta\hat{e}_z \times \mathbf{V}^p = 0, \tag{18}$$

$$\frac{\partial\theta}{\partial t} + (\mathbf{V}^f + \mathbf{V}^p) \cdot \nabla\theta = (\mathbf{w}^f + \mathbf{w}^p) + \nabla^2\theta, \tag{19}$$

$$\epsilon_1 Le \frac{\partial\phi}{\partial t} + A Le (\mathbf{V}^f + \mathbf{V}^p) \cdot \nabla\phi = (\mathbf{w}^f + \mathbf{w}^p) + \nabla^2\phi + S\nabla^2\theta, \tag{20}$$

$$\mathbf{w}^f = \mathbf{w}^p = \theta = \phi = 0 \text{ on } z = 0, 1. \tag{21}$$

By taking the third component of curl of Equations (17) and (18), one obtains

$$\mathbf{w}_3^f + \gamma(\mathbf{w}_3^f - \mathbf{w}_3^p) - Ta \frac{\partial\mathbf{w}^f}{\partial z} = 0, \tag{22}$$

$$\kappa_r\mathbf{w}_3^p + \gamma(\mathbf{w}_3^p - \mathbf{w}_3^f) - \eta Ta \frac{\partial\mathbf{w}^p}{\partial z} = 0, \tag{23}$$

where $D = \frac{\partial}{\partial t}, \mathbf{w}_3^f = \frac{\partial v^f}{\partial x} - \frac{\partial u^f}{\partial y}$.

By taking the third component of double curl of Equations (17) and (18), one has

$$\nabla^2\mathbf{w}^f + \gamma(\nabla^2\mathbf{w}^f - \nabla^2\mathbf{w}^p) - R\nabla_h^2\theta + R_C\nabla_h^2\phi + Ta \frac{\partial\mathbf{w}_3^f}{\partial z} = 0, \tag{24}$$

$$\kappa_r\nabla^2\mathbf{w}^p + \gamma(\nabla^2\mathbf{w}^p - \nabla^2\mathbf{w}^f) - R\nabla_h^2\theta + R_C\nabla_h^2\phi + \eta Ta \frac{\partial\mathbf{w}_3^p}{\partial z} = 0, \tag{25}$$

where

$$\nabla_h^2 = \frac{\partial^2}{\partial x^2} + \frac{\partial^2}{\partial y^2}$$

and

$$\nabla^2 = \frac{\partial^2}{\partial x^2} + \frac{\partial^2}{\partial y^2} + \frac{\partial^2}{\partial z^2}.$$

Solving Equations (22) and (23) with respect to \mathbf{w}_3^f and \mathbf{w}_3^p , respectively, one has

$$\mathbf{w}_3^f = \frac{Ta(\gamma + \kappa_r)\mathbf{w}_z^f + \eta Ta\gamma\mathbf{w}_z^p}{\gamma + \kappa_r + \gamma\kappa_r}, \tag{26}$$

$$\mathbf{w}_3^p = \frac{Ta(\gamma\mathbf{w}_z^f) + \eta Ta(1 + \gamma)\mathbf{w}_z^p}{\gamma + \kappa_r + \gamma\kappa_r}. \tag{27}$$

Substituting Equations (26) and (27) into Equations (24) and (25), respectively, one obtains

$$\nabla^2 \mathbf{w}^f + \gamma (\nabla^2 \mathbf{w}^f - \nabla^2 \mathbf{w}^p) - R \nabla_h^2 \theta + R_C \nabla_h^2 \phi + \frac{Ta^2(\gamma + \kappa_r) \mathbf{w}_{zz}^f + \eta Ta^2 \gamma \mathbf{w}_{zz}^p}{\gamma + \kappa_r + \gamma \kappa_r} = 0, \tag{28}$$

$$\kappa_r \nabla^2 \mathbf{w}^p + \gamma (\nabla^2 \mathbf{w}^p - \nabla^2 \mathbf{w}^f) - R \nabla_h^2 \theta + R_C \nabla_h^2 \phi + \frac{\eta Ta^2 \gamma \mathbf{w}_{zz}^f + \eta^2 Ta^2 (1 + \gamma) \mathbf{w}_{zz}^p}{\gamma + \kappa_r + \gamma \kappa_r} = 0. \tag{29}$$

Hence, considering Equations (19), (20), (28) and (29), we see the following problem in $\mathbf{w}^f, \mathbf{w}^p, \theta$, and ϕ :

$$\nabla^2 \mathbf{w}^f + \gamma (\nabla^2 \mathbf{w}^f - \nabla^2 \mathbf{w}^p) - R \nabla_h^2 \theta + R_C \nabla_h^2 \phi + \frac{Ta^2(\gamma + \kappa_r) \mathbf{w}_{zz}^f + \eta Ta^2 \gamma \mathbf{w}_{zz}^p}{\gamma + \kappa_r + \gamma \kappa_r} = 0, \tag{30}$$

$$\kappa_r \nabla^2 \mathbf{w}^p + \gamma (\nabla^2 \mathbf{w}^p - \nabla^2 \mathbf{w}^f) - R \nabla_h^2 \theta + R_C \nabla_h^2 \phi + \frac{\eta Ta^2 \gamma \mathbf{w}_{zz}^f + \eta^2 Ta^2 (1 + \gamma) \mathbf{w}_{zz}^p}{\gamma + \kappa_r + \gamma \kappa_r} = 0, \tag{31}$$

$$\frac{\partial \theta}{\partial t} = \mathbf{w}^f + \mathbf{w}^p + \nabla^2 \theta, \tag{32}$$

$$\varepsilon_1 L e \frac{\partial \phi}{\partial t} = \mathbf{w}^f + \mathbf{w}^p + \nabla^2 \phi + S \nabla^2 \theta. \tag{33}$$

3. Linear Stability Analysis

Let us consider the normal mode solutions in the form of

$$(\mathbf{w}^f, \mathbf{w}^p, \theta, \phi) = (w^f, w^p, \theta, \phi) \sin(n\pi z) e^{i(lx + my) + \sigma t}. \tag{34}$$

Substituting the above normal mode solution into the Equations (30)–(33), we find

$$[A\Lambda(1 + \gamma) + n^2 \pi^2 Ta^2 B] \mathbf{w}^f + [\eta \gamma n^2 \pi^2 Ta^2 - \gamma \Lambda A] \mathbf{w}^p - a^2 RA\theta + a^2 R_C A\phi = 0, \tag{35}$$

$$[\eta \gamma n^2 \pi^2 Ta^2 - \gamma \Lambda A] \mathbf{w}^f + [\Lambda AB + \eta^2 n^2 \pi^2 Ta^2 (1 + \gamma)] \mathbf{w}^p - a^2 RA\theta + a^2 R_C A\phi = 0, \tag{36}$$

$$\mathbf{w}^f + \mathbf{w}^p + [\sigma - \Lambda] \theta = 0, \tag{37}$$

$$\mathbf{w}^f + \mathbf{w}^p - S\Lambda\theta - [\varepsilon_1 L e \sigma + \Lambda] \phi = 0, \tag{38}$$

where

$$\begin{cases} a^2 = l^2 + m^2 \text{ is the wave number,} \\ \sigma = i\omega, \\ A = \gamma + \kappa_r + \gamma \kappa_r, \\ B = \gamma + \kappa_r, \\ \Lambda = \pi^2 + a^2. \end{cases}$$

Requiring zero determinant of the above system, one has

$$R = \frac{\xi_1 + \omega^2 \xi_2 + i(\xi_3 + \omega^2 \xi_4)}{\xi_5}, \tag{39}$$

with

$$\begin{cases} \xi_1 = \Lambda^2[-a^2\Lambda R_C(S-1)(x_1 + A\Lambda(1+B+3\gamma)) + \Lambda(x_2 + x_3\Lambda + x_4\Lambda^2)], \\ \xi_2 = x[a^2AR_C(x_1 + A\Lambda(1+B+3\gamma)) + x\Lambda(x_2 + x_3\Lambda + x_4\Lambda^2)], \\ \xi_3 = a^2A\Lambda R_C(1-x+Sx)[x_1 + A\Lambda(1+B+3\gamma)] + \Lambda^2[x_2 + x_3\Lambda + x_4\Lambda^2], \\ \xi_4 = x^2(x_2 + x_3\Lambda + x_4\Lambda^2), \\ \xi_5 = a^2A(\omega^2x^2 + \Lambda^2)[\pi^2Ta^2(B + \eta(\gamma\eta - 2\gamma + \eta)) + A\Lambda(1+B+3\gamma)], \\ x_1 = \pi^2Ta^2(B + \eta^2 + \eta^2\gamma - 2\eta\gamma), \\ x_2 = \pi^4Ta^4(B + B\gamma - \gamma^2)\eta^2, \\ x_3 = A\pi^2Ta^2(B^2 + 2\eta\gamma^2 + (1 + \gamma^2)\eta^2), \\ x_4 = A^2(B + B\gamma - \gamma^2), \\ x = Le\varepsilon_1. \end{cases}$$

3.1. Stationary Convection:

Substituting $\omega = 0$ in Equation (39), one obtains

$$R_{T_{sc}} = \frac{\xi_6 + \xi_7\Lambda + \xi_8\Lambda^2 + \xi_9\Lambda^3}{\xi_{10} + \xi_{11}\Lambda}, \tag{40}$$

where

$$\begin{cases} \xi_6 = a^2\pi^2Rc(1-S)Ta^2(\kappa_r + \gamma(-1 + \eta)^2 + \eta^2), \\ \xi_7 = a^2ARc(1-S)(1+k+4\gamma) + \pi^4Ta^4\eta^2, \\ \xi_8 = \pi^2Ta^2((\kappa_r + \gamma)^2 + 2\eta\gamma^2 + (1 + \gamma)^2\eta^2), \\ \xi_9 = A^2, \\ \xi_{10} = a^2\pi^2Ta^2(\kappa_r + \gamma(-1 + \eta)^2 + \eta^2), \\ \xi_{11} = a^2A(1+k+4\gamma). \end{cases}$$

In the absence of rotation and the Soret effect, the above-stationary Rayleigh number reduces to

$$Ra_{sc} = \frac{\delta^4(\gamma + \kappa_r + \gamma\kappa_r)}{q^2(1 + \kappa_r + 4\gamma)}, \tag{41}$$

which, on comparison, satisfies [16] (Equation (31)).

The case of a monodisperse porous layer rotating about a vertical axis with the Darcy model has been considered in Capone and Rionero [32]. As $\kappa_r \rightarrow \infty$, $\gamma \rightarrow 0$, $Rc \rightarrow 0$, and $\eta \rightarrow \infty$ in Equation (40), we find

$$Ra_{sc} = \frac{\delta^2(\pi^2Ta^2 + \delta^2)}{q^2}. \tag{42}$$

After some calculations, we find

$$Ra_{scl} = \pi^2(1 + \sqrt{1 + Ta^2})^2, \tag{43}$$

which is in good agreement with [32] (Equation (4.24), p. 195).

3.2. Oscillatory Convection

To study the oscillatory stability, we consider the real and imaginary parts of R . The Rayleigh number at the onset of oscillatory convection is

$$R_{T_{oc}} = \frac{\xi_{12} + \xi_{13}\Lambda + \xi_{14}\Lambda^2 + \xi_{15}\Lambda^3}{\xi_{16} + \xi_{17}\Lambda}, \tag{44}$$

where

$$\begin{cases} \tilde{\xi}_{12} = a^2 \pi^2 R_C T a^2 (\kappa_r + \gamma(-1 + \eta)^2 + \eta^2), \\ \tilde{\xi}_{13} = a^2 A R_C (1 + k + 4\gamma) + \pi^4 T a^4 (1 + x) \eta^2, \\ \tilde{\xi}_{14} = \pi^2 T a^2 (1 + x) ((\kappa_r + \gamma)^2 + 2\eta\gamma^2 + (1 + \gamma)^2 \eta^2), \\ \tilde{\xi}_{15} = (1 + x) A^2, \\ \tilde{\xi}_{16} = x a^2 \pi^2 T a^2 (\kappa_r + \gamma(-1 + \eta)^2 + \eta^2), \\ \tilde{\xi}_{17} = x a^2 A (1 + k + 4\gamma). \end{cases}$$

4. Discussion

The numerical results and discussions are presented in this section. The critical Rayleigh number at the onset of stationary convection, $Ra_{T_{sc}}^c$; at the onset of oscillatory convection, $Ra_{T_{oc}}^c$; the critical wave number at the onset of stationary convection, q_{sc}^c ; and at the onset of oscillatory convection, q_{oc}^c , are obtained for the prescribed values of other parameters. Figures 2–8 show the neutral curves in the parametric plane (q, R_T) with different values of the Ta, S, R_C , and κ_r .

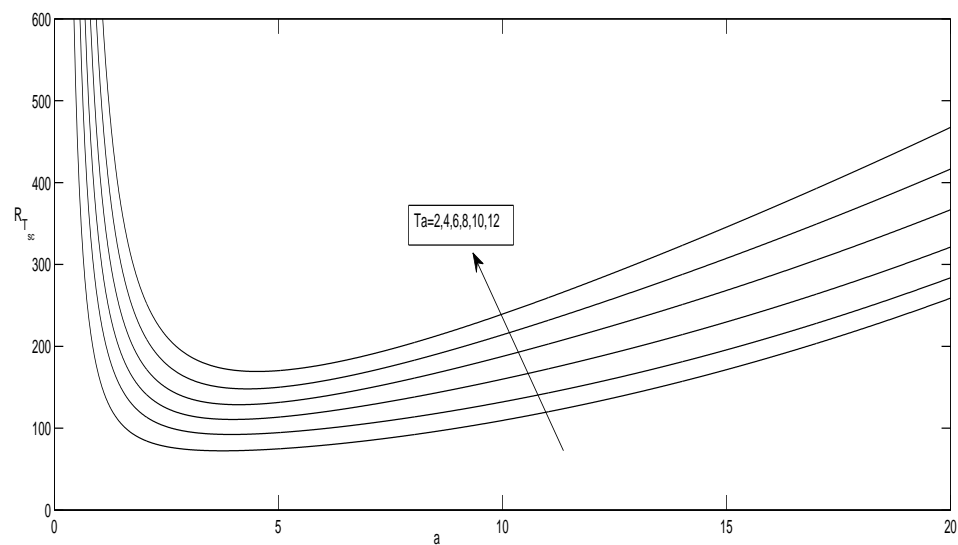


Figure 2. Neutral curves for the different values of Ta and for the fixed values of $\gamma = 0.5, \eta = 0.2, \kappa_r = 1, R_C = 50$, and $S = 0.5$ for the stationary mode.

In the stationary mode, the neutral curves are displayed in Figures 2–5. Figure 2 shows the neutral curves in the parametric plane (q, R_T) with different values of the Taylor number. From this figure, one can observe that, as Ta increases, the curves shift upward, indicating a delay in the onset of instability. This can be explained as follows: Vorticity is introduced into the fluid when it rotates. As a result, the fluid travels faster in horizontal planes. The velocity of the fluid perpendicular to the planes decreases as a result of this motion, therefore $Ra_{T_{sc}}^c$ rises with Ta .

The effect of the Soret parameter on the onset of instability is shown in Figure 3. In it, we see that $R_{T_{sc}}^c$ decreases with the Soret parameter, which means that the Soret parameter destabilizes the system. For various values of solute Rayleigh number, with changing values of wave number and then Rayleigh numbers, the neutral curves are obtained in Figure 4. We can see from this figure that $R_{T_{sc}}^c$ increases as R_C increases, indicating that the presence of R_C suppresses the onset of convection.

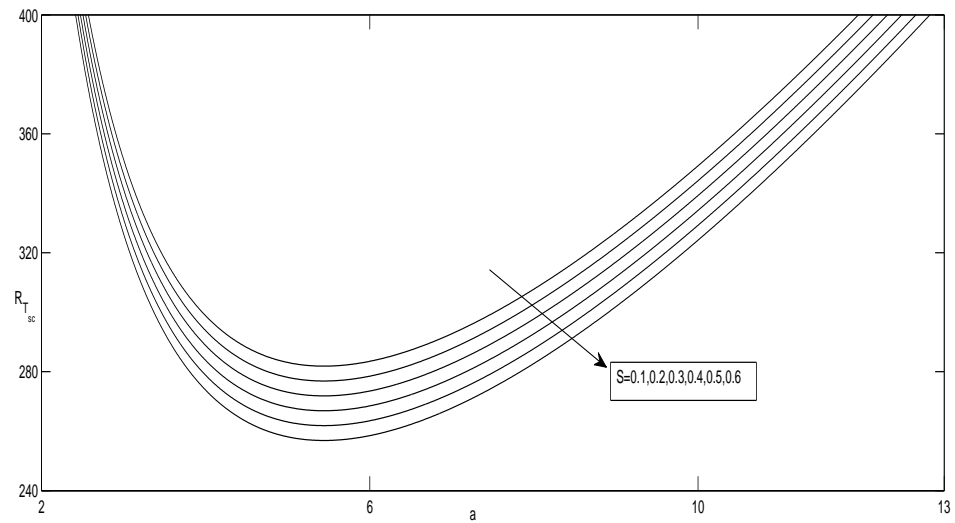


Figure 3. Neutral curves for the different values of S and for the fixed values of $\gamma = 0.5$, $\eta = 0.2$, $\kappa_r = 1$, $R_C = 50$, and $Ta = 20$ for the stationary mode.

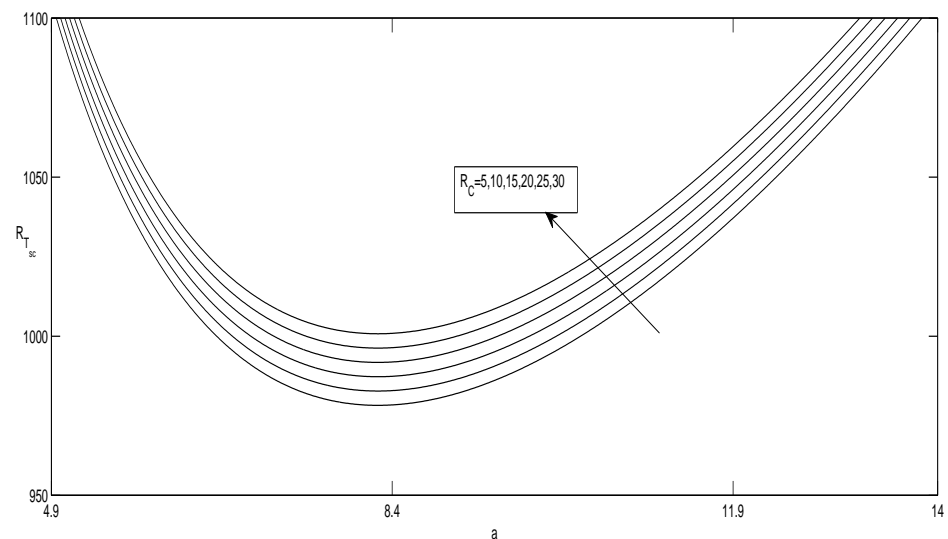


Figure 4. Neutral curves for the different values of R_C and for the fixed values of $\gamma = 0.5$, $\eta = 0.2$, $\kappa_r = 1$, $S = 0.2$, and $Ta = 50$ for the stationary mode.

Figure 5 depicts the neutral curves at the onset of stationary convection for various values of κ_r . According to this figure, $R_{T_{sc}}^c$ decreases as κ_r increases, indicating that the presence of a solute Rayleigh number advances the onset of convection. The neutral curves at the onset of oscillatory convection are displayed in Figures 6–8. Figure 6 displays the neutral curves for different values of Ta . According to this figure, increasing Ta causes $R_{T_{oc}}^c$ to increase, indicating that Ta has the effect of stabilizing the system.

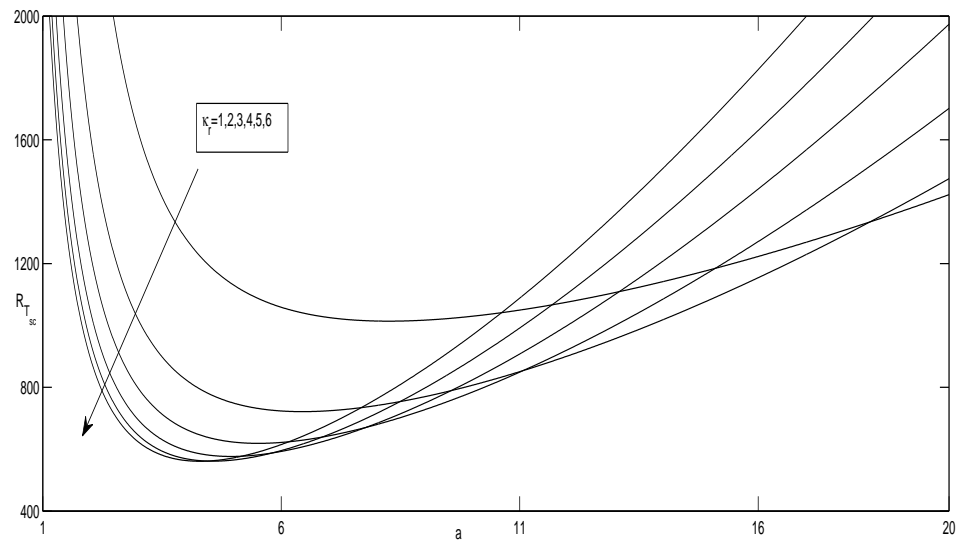


Figure 5. Neutral curves for the different values of κ_r and for the fixed values of $\gamma = 0.5, \eta = 0.2, R_C = 50, S = 0.2,$ and $Ta = 50$ for the stationary mode.

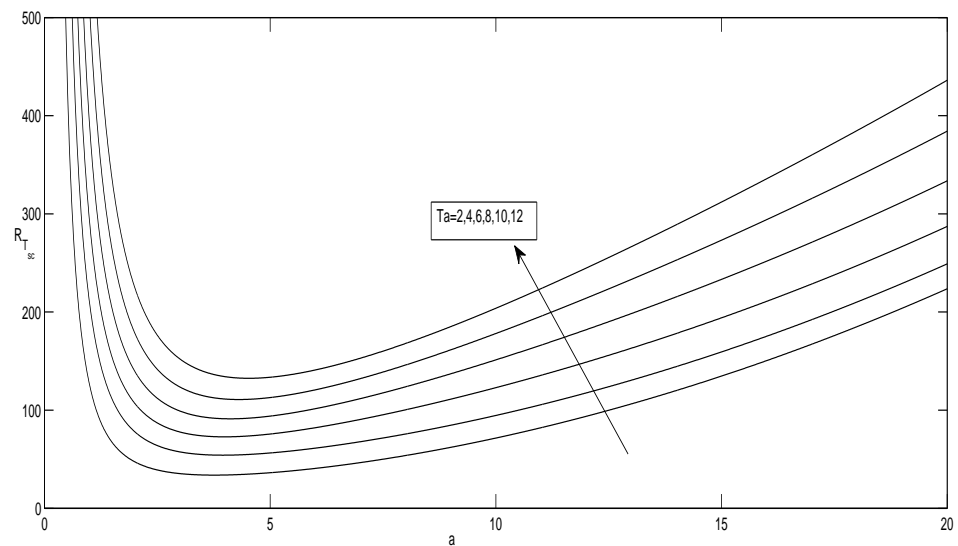


Figure 6. Neutral curves for the different values of Ta and for the fixed values of $\gamma = 0.5, \eta = 0.2, R_C = 50,$ and $\kappa_r = 1$ for the oscillatory mode.

Figure 7 depicts the neutral curves for different values of R_C at the onset of oscillatory convection, and it is found that the neutral curves move upward with an increase in the value of R_C , thus R_C stabilizes the oscillatory convection.

Figure 8 shows the effect of κ_r . In particular, we observe that the effect of κ_r advances the onset of convection. This can be understandable, mathematically, because $\kappa_r = \frac{\kappa_f}{\kappa_p}$, κ_r increases as κ_p decreases (κ_f is assumed to be fixed here). In other words, as microporosity declines, fluid movement in micropores becomes more difficult. As a result, convective motions become more difficult, yielding more stability to the system.

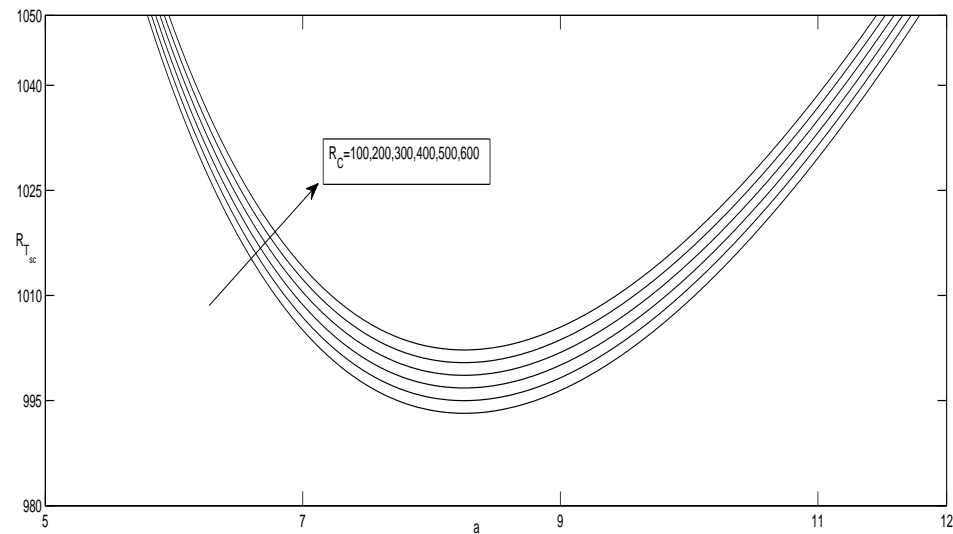


Figure 7. Neutral curves for the different values of R_C and for the fixed values of $\gamma = 0.5, \eta = 0.2, Ta = 50,$ and $\kappa_r = 1$ for the oscillatory mode.

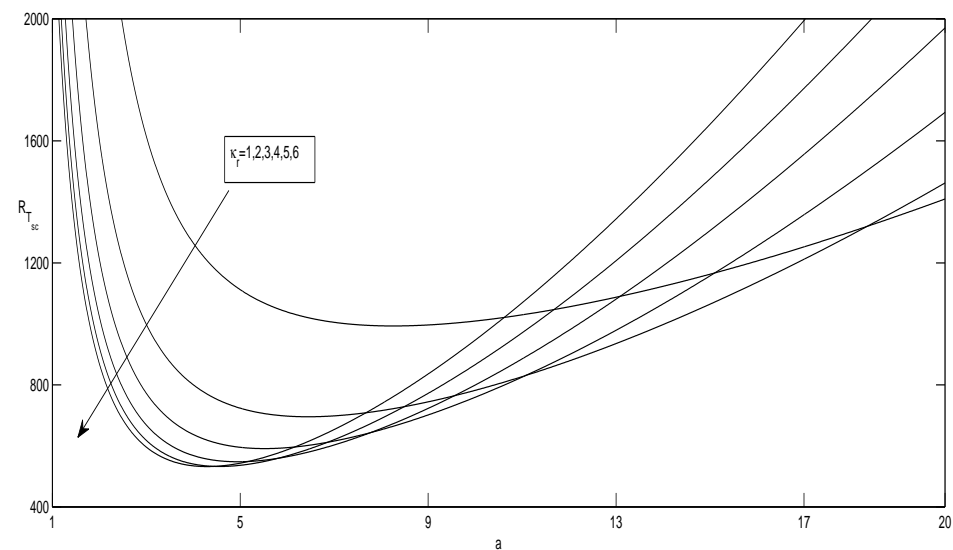


Figure 8. Neutral curves for the different values of $\kappa_r,$ and for the fixed values of $\gamma = 0.5, \eta = 0.2, Ta = 50$ and $R_C = 100$ for the oscillatory mode.

In Tables 1–3, we present some examples in which steady or oscillatory instability sets in for the constant values of physical parameters. According to Table 1, there is a threshold $R_C^* (\in 0.45, 0.46)$ for the solute Rayleigh number, such that, if $R_C > R_C^*$, then the convection arises via an oscillatory mode. According to Table 2, oscillatory convection occurs initially, and as soon as the value of S reaches a critical value ($\in (0.6, 0.7)$), the convection ceases to be oscillatory, and stationary convection occurs as the first bifurcation. Table 3 shows that, as the value of κ_r increases, convection always occurs via stationary mode.

Table 1. Critical stationary and oscillatory Rayleigh numbers for different values of R_c and the fixed values of $\kappa_r = 1$, $Ta = 5$, and $S = 0.5$.

R_c	Stationary R	Stationary a	Oscillatory R	Oscillatory a	Instability
0	61.6464	3.9578	62.7612	3.9578	Stationary
1	62.1464	3.9578	62.7793	3.9578	Stationary
2	62.6464	3.9578	62.7973	3.9578	Stationary
3	63.1464	3.9578	62.8154	3.9578	Oscillatory
4	63.6464	3.9578	62.8335	3.9578	Oscillatory
5	64.1464	3.9578	62.8516	3.9578	Oscillatory

Table 2. Critical stationary and oscillatory Rayleigh numbers for the different values of S and the fixed values of $\kappa_r = 1$, $Ta = 50$, and $R_c = 50$.

S	Stationary R	Stationary a	Oscillatory R	Oscillatory a	Instability
0.1	1018.7706	8.2527	992.2842	8.2527	Oscillatory
0.2	1013.7706	8.2527	992.2842	8.2527	Oscillatory
0.3	1008.7706	8.2527	992.2842	8.2527	Oscillatory
0.4	1003.7706	8.2527	992.2842	8.2527	Oscillatory
0.5	998.7706	8.2527	992.2842	8.2527	Oscillatory
0.6	993.7706	8.2527	992.2842	8.2527	Oscillatory
0.7	988.7706	8.2527	992.2842	8.2527	Stationary
0.8	983.7706	8.2527	992.2842	8.2527	Stationary
0.9	978.7706	8.2527	992.2842	8.2527	Stationary

Table 3. Critical stationary and oscillatory Rayleigh numbers for the different values of κ_r and the fixed values of $S = 0.8$, $Ta = 50$, and $R_c = 50$.

κ_r	Stationary R	Stationary a	Oscillatory R	Oscillatory a	Instability
1	983.7706	8.2540	992.2842	8.2540	Stationary
2	691.3454	6.4421	694.5709	6.4421	Stationary
3	588.8136	5.5171	590.1849	5.5171	Stationary
4	546.4455	4.9469	547.0506	4.9469	Stationary
5	531.2631	4.5668	531.5936	4.5668	Stationary

5. Conclusions

In this study, we investigated the onset of rotating convection in a horizontal bidisperse porous layer that is uniformly heated and salted from below. The behaviour of various parameters, such as the Ta , S , R_c , and κ_r , has been analysed. The results can be summarized as follows:

- $R_{T_{sc}}^c$ and $R_{T_{oc}}^c$ increase as the Taylor number increases, indicating that Ta has a stabilizing effect on the onset of convection.
- $R_{T_{sc}}^c$ and $R_{T_{oc}}^c$ are increasing functions of R_c and decreasing functions of κ_r .
- S does not show any effect on $R_{T_{oc}}^c$, as $R_{T_{oc}}^c$ is independent of S .
- There exists a threshold $R_c^* \in (0.45, 0.46)$ for the solute Rayleigh number such that, if $R_c > R_c^*$, then the convection arises via an oscillatory mode.
- The oscillatory convection sets in and, as soon as the value of S attains a critical value ($\in (0.6, 0.7)$), the convection ceases to be oscillatory, and stationary convection occurs as the first bifurcation.

Author Contributions: Conceptualization, C.R. and G.S.K.R.; methodology, C.R.; software, C.R.; validation, C.R., N.K., G.S.K.R., K.K.P. and C.C.; formal analysis, C.R.; investigation, C.R.; data curation, C.R.; writing—original draft preparation, C.R.; writing—review and editing, C.R., N.K., G.S.K.R., K.K.P. and C.C.; visualization, C.R.; supervision, G.S.K.R., N.K., K.K.P. and C.C. All authors have read and agreed to the published version of the manuscript.

Funding: This research received no external funding.

Acknowledgments: The authors would like to thank the reviewers for their insightful comments on the paper.

Conflicts of Interest: The authors declare no conflict of interest.

Nomenclature

C_a	Acceleration coefficient
κ_f	Permeability in macro pores
κ_p	Permeability in micro pores
ζ	Interaction coefficient
μ	Fluid viscosity
g	Gravity
α	Coefficient of thermal expansion
α_c	Density coefficient for salinity
σ	Heat capacity ratio
ϵ	Macro porosity
δ	Micro porosity
ρ	Density
k_s	Thermal conductivity of the solid
k_f	Thermal conductivity of the fluid
$(\rho c)_s$	Product of density and specific heat in the solid skeleton
$(\rho c)_f$	Product of density and specific heat in the pores
ρ_0	Reference density
k_m	Thermal conductivity
p^f	Pressure in macro pores
p^p	Pressure in micro pores
T	Temperature
C	Salt concentration field
R	Rayleigh number
R_C	Solutal Rayleigh number
Ta	Taylor number
Le	Lewis number
S	Soret number
d	Length
Superscripts	
'	Perturbated quantity
c	Critical value
Subscripts	
b	Base state
0	Reference valve

References

- Chen, Z.Q.; Cheng, P.; Hsu, C.T. A theoretical and experimental study on stagnant thermal conductivity of bi-dispersed porous media. *Int. Commun. Heat Mass Transf.* **2000**, *27*, 601–610. [[CrossRef](#)]
- Chen, Z.Q.; Cheng, P.; Zhao, T.S. An experimental study of two phase flow and boiling heat transfer in bi-disperse porous channels. *Int. Commun. Heat Mass Transf.* **2000**, *27*, 293–302. [[CrossRef](#)]
- Gérard, A.; Genter, A.; Kohl, T.; Lutz, P.; Rose, P.; Rummel, F. The deep EGS (Enhanced Geothermal System) project at Soultz-sous-Forêts (Alsace, France). *Geothermics* **2006**, *35*, 473–483. [[CrossRef](#)]
- Nie, R.S.; Meng, Y.F.; Jia, Y.L.; Zhang, F.X.; Yang, X.T.; Niu, X.N. Dual porosity and dual permeability modeling of horizontal well in naturally fractured reservoir. *Transp. Porous Med.* **2012**, *92*, 213–235. [[CrossRef](#)]
- Nield, D.; Kuznetsov, A. Forced convection in a bidisperse porous medium channel: A conjugate problem. *Int. J. Heat Mass Transf.* **2004**, *47*, 53755380. [[CrossRef](#)]
- Nield, D.; Kuznetsov, A. A two-velocity two-temperature model for a bidispersed porous medium: Forced convection in a channel. *Transp. Porous Media* **2005**, *59*, 325339. [[CrossRef](#)]
- Nield, D.A.; Kuznetsov, A.V. The onset of convection in a bidispersive porous medium. *Int. J. Heat Mass Transf.* **2006**, *49*, 3068–3074. [[CrossRef](#)]

8. Nield, D.; Kuznetsov, A. A note on modeling high speed flow in a bidisperse porous medium. *Transp. Porous Media* **2013**, *96*, 495499. [[CrossRef](#)]
9. Nield, D.; Kuznetsov, A. The effect of combined vertical and horizontal heterogeneity on the onset of convection in a bidisperse porous medium. *Int. J. Heat Mass Transf.* **2007**, *50*, 33293339. [[CrossRef](#)]
10. Nield, D.; Kuznetsov, A. Natural convection about a vertical plate embedded in a bidisperse porous medium. *Int. J. Heat Mass Transf.* **2008**, *51*, 16581664. [[CrossRef](#)]
11. Nield, D.; Kuznetsov, A. Forced convection in a channel partly occupied by a bidisperse porous medium: Symmetric case. *J. Heat Transf.* **2011**, *133*, 072601. [[CrossRef](#)]
12. Kuznetsov, A.V.; Nield, D. Thermally developing forced convection in a bidisperse porous medium. *J. Porous Media* **2006**, *9*, 393402.
13. Straughan, B. On the NieldKuznetsov theory for convection in bidispersive porous media. *Transp. Porous Media* **2009**, *77*, 159168 [[CrossRef](#)]
14. Straughan, B. *Convection with Local Thermal NonEquilibrium and Microfluidic Effects*; Springer: Berlin/Heidelberg, Germany, 2015.
15. Falsaperla, P.; Mulone, G.; Straughan, B. Bidispersiveinclined convection. *Proc. R. Soc. A* **2016**, *472*, 20160480. [[CrossRef](#)] [[PubMed](#)]
16. Gentile, M.; Straughan, B. Bidispersive thermal convection. *Int. J. Heat Mass Transf.* **2017**, *114*, 837840. [[CrossRef](#)]
17. Gentile, M.; Straughan, B. Bidispersive vertical convection. *Proc. R. Soc. A* **2017**, *473*, 20170481. [[CrossRef](#)]
18. Capone, F.; De Luca, R.; Gentile, M. Coriolis effect on thermal convection in a rotating bidispersive porous layer. *Proc. R. Soc. A* **2020**, *476*, 20190875. [[CrossRef](#)]
19. Capone, F.; De Luca, R. The Effect of the Vadasz Number on the Onset of Thermal Convection in Rotating Bidispersive Porous Media. *Fluids* **2020**, *5*, 173. [[CrossRef](#)]
20. Rionero, S. Onset of convection in porous layers salted from above and below. *Note Mat.* **2012**, *32*, 159173.
21. Rionero, S. Global nonlinear stability for a triply diffusive convection in a porous layer. *Contin. Mech. Thermodyn.* **2012**, *24*, 629641. [[CrossRef](#)]
22. Rionero, S. Triple diffusive convection in porous media. *Acta Mech.* **2013**, *224*, 447458. [[CrossRef](#)]
23. Iasiello, M.; Vafai, K.; Andreozzi, A.; Bianco, N. Hypo- and hyperthermia effects on LDL deposition in a curved artery. *Comput. Therm. Sci. Int. J.* **2019**, *11*, 95–103. [[CrossRef](#)]
24. Iasiello, M.; Vafai, K.; Andreozzi, A.; Bianco, N. Low-density lipoprotein transport through an arterial wall under hyperthermia and hypertension conditions—An analytical solution. *J. Biomech.* **2016**, *49*, 193–204. [[CrossRef](#)] [[PubMed](#)]
25. Maiti, S.; Shaw, S.; Shit, G.C. Fractional order model for thermochemical flow of blood with Dufour and Soret effects under magnetic and vibration environment. *Colloids Surf. Biointerfaces* **2021**, *197*, 111395. [[CrossRef](#)] [[PubMed](#)]
26. Reddy, G.S.K.; Ragoju, R. Thermal instability of a Maxwell fluid saturated porous layer with chemical reaction. *Spec. Top. Rev. Porous Media Int. J.* **2022**, *13*, 33–47. [[CrossRef](#)]
27. Babu, A.B.; Reddy, G.S.K.; Tagare, S.G. Nonlinear magneto convection due to horizontal magnetic field and vertical axis of rotation due to thermal and compositional buoyancy. *Results Phys.* **2019**, *12*, 2078–2090. [[CrossRef](#)]
28. Benerji, Babu, A.; Reddy, G.S.K.; Tagare, S.G. Nonlinear magnetoconvection in a rotating fluid due to thermal and compositional buoyancy with anisotropic diffusivities. *Heat Transf. Asian Res.* **2020**, *49*, 335–355. [[CrossRef](#)]
29. Straughan, B. Bidispersive double diffusive convection. *Int. J. Heat Mass Transf.* **2018**, *126*, 504–508. [[CrossRef](#)]
30. Straughan, B. Effect of inertia on double diffusive bidispersive convection. *Int. J. Heat Mass Transf.* **2019**, *129*, 389–396. [[CrossRef](#)]
31. Badday, A.J.; Harfash, A.J. Double-diffusive convection in bidispersive porous medium with chemical reaction and magnetic field effects. *Transp. Porous Media* **2021**, *139*, 45–66. [[CrossRef](#)]
32. Capone, F.; Rionero, S. Inertia effect on the onset of convection in rotating porous layers via the auxiliary system method. *Int. J. Nonlinear Mech.* **2013**, *57*, 192–200. [[CrossRef](#)]